Brashler, J. R., Bach, M. K., & Askenase, P. W. (1984) *J. Immunol. 132*, 1993–1999.
Rola-Pleszczynski, M., & Lemaire, I. (1985) *J. Immunol. 135*, 3958–3961.
Rouzer, C. A., Scott, W. A., Hamill, A. L., & Cohn, Z. A. (1980) *J. Exp. Med. 152*, 1236–1244.
Rouzer, C. A., Scott, W. A., Hamill, A. L., Liu, F.-T., Katz, D. H., & Cohn, Z. A. (1982) *J. Exp. Med. 156*, 1077–1086.
Samuelsson, B. (1983) *Science (Washington, D.C.) 220*, 568–575.
Snyder, D. W., & Krell, R. D. (1984) *J. Pharmacol. Exp. Ther. 231*, 616–622.
Sun, F. F., chan, L. Y., Spurr, B., Corey, E. J., Lewis, R. A., & Austen, K. F. (1986) *J. Biol. Chem. 261*, 8540–8546.
Williams, J. D., Czop, J. L., & Austen, K. F. (1984) *J. Immunol. 132*, 3034–3040.

# X-ray Diffraction Study of the Polymorphic Behavior of N-Methylated Dioleoylphosphatidylethanolamine†

S. M. Gruner,* M. W. Tate, G. L. Kirk,‡ P. T. C. So, D. C. Turner, and D. T. Keane
*Department of Physics, Princeton University, Princeton, New Jersey 08544*
C. P. S. Tilcock and P. R. Cullis
*Department of Biochemistry, University of British Columbia, Vancouver V6T 1W5, Canada*
*Received February 27, 1987; Revised Manuscript Received November 6, 1987*

ABSTRACT: The polymorphic phase behavior of aqueous dispersions of dioleoylphosphatidylethanolamine (DOPE) and its N-methylated analogues, DOPE-Me, DOPE-$Me_2$, and DOPC, has been investigated by X-ray diffraction. In the fully hydrated lamellar ($L_\alpha$) phase at 2 °C, the major structural difference is a large increase in the interlamellar water width from DOPE to DOPE-Me, with minor increases with successive methylation. Consistent with earlier reports, inverted hexagonal ($H_{II}$) phases are observed upon heating at 5–10 °C in DOPE and at 65–75 °C in DOPE-Me and are not observed to at least 85 °C in DOPE-$Me_2$ or DOPC. In DOPE, the $L_\alpha$–$H_{II}$ transition is facile and is characterized by a relatively narrow temperature range of coexistence of $L_\alpha$ and $H_{II}$ domains, each with long-range order. DOPE-Me exhibits complex nonequilibrium behavior below the occurrence of the $H_{II}$ phase: Upon heating, the $L_\alpha$ lattice spontaneously disorders on a time scale of days; on cooling from the $H_{II}$ phase, the disorder rises on a time scale of minutes. It is shown that, in copious water, the disordered state transforms very slowly into phases with cubic symmetry. This process is assisted by the generation of small amounts of lipid degradation products. The relative magnitudes of the monolayer spontaneous radius of curvature, $R_0$ [Kirk, G. L., Gruner, S. M., & Stein, D. L. (1984) *Biochemistry 23*, 1093; Gruner, S. M. (1985) *Proc. Natl. Acad. Sci. U.S.A. 82*, 3665], are inferred from the $H_{II}$ lattice spacings vs temperature and are shown to increase with increasing methylation. The relative magnitudes of $R_0$ are categorized as small for DOPE, intermediate for DOPE-Me, and large for DOPC. It is suggested, and examples are used to illustrate, that small $R_0$ lipid systems exhibit facile, low-temperature $L_\alpha$–$H_{II}$ transitions, intermediate $R_0$ systems exhibit complex nonequilibrium transition behavior and are likely to form cubic phases, and large $R_0$ systems are stable as $L_\alpha$ phases. The relationship between the cubic phases and minimal periodic surfaces is discussed. It is suggested that minimal periodic surfaces represent geometries in which near constant, intermediate $R_0$ values can be obtained concomitantly with monolayers of near constant thickness, thereby leading to equilibrium cubic phases. Thus, the relative magnitude of the spontaneous radius of curvature may be used to predict mesomorphic behavior. The geometry of the equilibrium phases that occur may be largely understood on the basis of a competition between a spontaneous tendency for the monolayers to curl to a radius, $R_0$, and the need to pack similar hydrocarbon chains at near constant density and at a uniform mean length.

An outstanding problem of membrane biology is to understand the roles of the numerous lipid species typically found in biomembranes (Raetz, 1982). The realization that large fractions of these lipid species do not individually form bilayers under physiological conditions [see Cullis et al. (1985) for a review] has focused much attention on the mesomorphic behavior of lipid liquid crystals (Gruner et al., 1985). A number of questions immediately arise: How do the so-called "nonbilayer" lipids affect the physical properties of the biological bilayers into which they are incorporated? What is the biological significance of these physical effects? What molecular characteristics determine the mesomorphic phase behavior of pure and mixed lipid systems? Are there readily measurable quantities that serve as predictors of classes of mesomorphic behavior?

One approach toward answering these questions is to attempt to understand the microscopic interactions present in lipid layers. Although an understanding of the molecular interactions is ultimately desirable, it is in practice, limited by the number and complexity of interatomic forces present in lipid–water dispersions. Moreover, the observation that chemically diverse lipids often exhibit similar mesomorphic behavior leads one to suspect that many complicated micro-

† This work was supported by the NIH (Grant GM32614), the DOE (Contract DE-FG02-87ER60522-A000), and the Medical Research Council (MRC) of Canada. P.R.C. is an MRC scientist. G.L.K. was additionally supported by the John B. Putman Foundation and M.W.T. by a Liposome Co. Fellowship.
* Author to whom correspondence should be addressed.
‡ Present address: 1000 Alegre Ave., Los Altos, CA 94022.

0006-2960/88/0427-2853$01.50/0 

scopic interactions lead to a few phenomenological parameters that dominate the system behavior. To draw an example by analogy, consider the behavior of metals. A great deal may be predicted about the macroscopic behavior of a metal if its tensile strength and electrical conductivity are known. Moreover, these phenomenological quantities can be measured and practically applied even if the microscopic sources are not understood. In this spirit, one seeks to identify phenomenological parameters from which one may predict the dominant mesomorphic behavior of lipids. An understanding of the microscopic sources of the phenomenological parameters is an important, but independent, line of inquiry.

Phosphatidylcholines (PCs)[1] and unsaturated phosphatidylethanolamines (PEs) are lipids that preferentially adopt, under physiological conditions, lamellar and nonlamellar phases, respectively. PC and PE head groups are identical except in the degree of methylation of the terminal quaternary nitrogen: In PE the nitrogen is bound to three hydrogens, whereas in PC each hydrogen has been replaced by a methyl group. This study reports on the mesomorphic behavior of dioleoylphosphatidylethanolamine (DOPE), dioleoylphosphatidylcholine (DOPC), and the two intermediates obtained by single (DOPE-Me) and double (DOPE-$Me_2$) methylation of the quaternary nitrogen. The theme of this study is to use X-ray diffraction to relate the structural dimensions of the lipid phases to a phenomenological parameter, the monolayer spontaneous radius of curvature, which has been shown to be a reliable predictor of mesomorphic behavior (Kirk, 1984; Kirk et al., 1984; Gruner, 1985; Kirk & Gruner, 1985; Tate & Gruner, 1987). This study complements a previously published report (Gagne et al., 1985) that primarily used DSC, NMR, and freeze-fracture electron microscopy to study N-methylated PEs. Some of the observations described herein were reported by Kirk (1984).

The purpose in emphasizing the relationship to a phenomenological parameter is that it allows categorization of classes of mesomorphic behavior along a continuum from highly nonbilayer prone to highly bilayer prone lipids. N-Methylated forms of DOPE represent points spaced on this continuum in which a particular microscopic variation, namely N-methylation, is used to alter the spontaneous radius of curvature. Other mechanisms of chemical modification, such as head-group ionization, glycosylation, or chain composition [see Cullis et al. (1985) and Gruner et al. (1985) for reviews] are also thought to alter the spontaneous radius. Although there is no attempt to perform an exhaustive examination of the universality of the connection between the classes of behavior exhibited by N-methylated DOPE and the relative values of the spontaneous radius, it is suggested that a general connection may exist and should be looked for. The existence of such a general connection would considerably simplify classification of the zoology of lipid mesomorphism. Moreover, as discussed below, connections of mesomorphic behavior to the spontaneous radius of curvature yield insight to the free energy contributions that dominate the phase transformations seen in lipid–water dispersions.

[1] Abbreviations: DAPE, diarachinoyl-PE; DGDG, diglucosyldiglyceride; DLPE, 1,2-dilauryl-*sn*-glycero-3-phosphoethanolamine; DOPC, 1,2-dioleoyl-*sn*-glycero-3-phosphocholine; DOPE, 1,2-dioleoyl-*sn*-glycero-3-phosphoethanolamine; DOPE-Me, 1,2-dioleoyl-*sn*-glycero-3-phospho-*N*-methylethanolamine; DOPE-$Me_2$, 1,2-dioleoyl-*sn*-glycero-3-phospho-*N*,*N*-dimethylethanolamine; DSC, differential scanning calorimetry; EDTA, ethylenediaminetetraacetic acid; HEPES, *N*-(2-hydroxyethyl)piperazine-*N*'-2-ethanesulfonic acid; MGDG, monoglucosyldiglyceride; NMR, nuclear magnetic resonance; PC, phosphatidylcholine; PE, phosphatidylethanolamine; PMS, periodic minimal surfaces; TLC, thin-layer chromatography.

## Materials and Methods

*Materials.* With the exception of the lipid used for Figure 5 and all experiments using DOPE-$Me_2$, data presented in this paper used commercially available lipid (Avanti Polar Lipids Birmingham, AL). DOPE-Me for Figure 5 and DOPE-$Me_2$ were prepared from DOPE by using the base exchange capacity of phospholipase D (Comfurius & Zwaal, 1977). The lipids were purified by preparative liquid chromatography on silica using $CHCl_3$/MeOH/$H_2O$ (60:30:2 v/v) as the mobile phase. Lipids were shown to be 1,2-diacyl-*sn*-glycero-3-phospho conformers on the basis of $^1H$ NMR, were greater than 99% pure with respect to lipid phosphorus as determined by phosphorus analysis following thin-layer chromatography, and were greater than 98% pure with respect to their fatty acid composition as determined by gas chromatography of their methyl esters. Results obtained with synthesized DOPE-Me and the commercial DOPE-Me were identical. Lipid purity was periodically checked via thin-layer chromatography (TLC). In cases where lipid degradation was observed, the degree of degradation was checked via gas chromatography or by comparison to calibration TLC plates of pure DOPE-Me to which known quantities of lysolipids and oleic acid had been added.

*X-ray Diffraction.* Nickel-filtered Cu K$\alpha$ (wavelength = 1.54 Å) X-rays were generated on a Rigaku RU-200 microfocus generator equipped with a 0.2 × 2 mm focus cup. X-rays were focused via Franks optics and recorded via image-intensified, slow scan, two-dimensional X-ray detectors as previously reported (Gruner, 1977; Milch, 1983; Reynolds et al., 1978; Gruner et al., 1982a,b). Unoriented lipid dispersions in glass capillaries, prepared as described below, were used in all diffraction experiments. The specimen temperature (±0.5 °C) during X-ray diffraction was controlled by a home-built, programmable, thermoelectrically servoed specimen stage with a rapid slew (~1 °C/s). For the measurement of lattice spacings vs temperature, the typical protocol involved stepwise heating the specimen at 5 °C/step, each step being followed by a 5–15 min thermal equilibration and an X-ray exposure of 1–4 min. Unusual thermal history protocols are described, as appropriate, in the figures and text. Figure 5 is derived from an exposure on Kodak (Rochester, NY) DEF X-ray film.

Data reduction of the two-dimensional powder-like diffraction patterns was performed by integrating circular arcs within, typically, ±10° of a line perpendicular to the long dimension of the incident X-ray beam (Gruner et al., 1982a,b). Integrations to either side of the beam stop are displayed separately. Because the analysis in this paper does not rely on precise measurements of the relative intensities of the diffracted orders, no correction for the ~20% nonuniformity of the detector response was applied. Typical absolute lattice spacings, calibrated against lead nitrate and dry lead stearate (long spacing = 47.5 Å at 20 °C), are accurate to ± 0.5 Å for lattices up to ~80 Å and to ±1 Å for larger lattices.

Bilayer and water dimensions in the $L_\alpha$ phase were determined by the method described by Luzzati (1968). The lipid volume fraction, $\phi$, is

$$\phi = [(1 + \bar{v}_w/\bar{v}_L)(1 - C)/C]^{-1}$$

where $C$ is the lipid weight fraction of the specimen and $\bar{v}_w$ and $\bar{v}_L$ are the partial specific volumes of water and lipid, respectively. The bilayer thickness, $d_B$, is

$$d_B = \phi d_L$$

Table I: Dimensions of Fully Hydrated N-Methylated DOPE Analogues[a]

| lipid | $T_c$ (°C) | $d_L$ (Å) | $C_L$ (wt %) | $d_W$ (Å) | $d_B$ (Å) | $S$ (Å$^2$) | $F_{HYD}$ ($\times 10^{-19}$ erg/Å$^3$) |
|---|---|---|---|---|---|---|---|
| DOPE | −5 to −10 | 52 | 70 ± 5 | 15 ± 3 | 37 ± 3 | 65 ± 5 | 8.5 |
| DOPE-Me | −10 to −15 | 61 | 63 ± 9 | 22 ± 5 | 39 ± 5 | 62 ± 8 | 2.6 |
| DOPE-Me$_2$ | −15 to −20 | 62 | 60 ± 3 | 25 ± 2 | 38 ± 2 | 66 ± 4 | 1.7 |
| DOPC | −15 to −20 | 61 | 59 ± 3 | 24 ± 2 | 36 ± 2 | 70 ± 4 | 1.9 |

[a] See Materials and Methods and Results for explanations of the symbols. All structural data were taken at 2 °C.

where $d_L$ is the lamellar repeat (X-ray long spacing). The area per lipid molecule, $S$, is

$$S = 2M\bar{v}_L/(d_B N_A)$$

where $M$ is the lipid molecular weight and $N_A$ is Avogadro's number.

For reasons that are not fully understood, the lamellar repeat, $d_L$, at near full hydration exhibited considerably less reproducibility than normally encountered with saturated chain lipids. This was especially true for DOPE-Me$_2$. Measurements of $d_L$ for the DOPE-Me$_2$ in distilled water were marked by broad, poorly formed lamellar peaks, time variation of $d_L$ even on sealed samples, and the presence of much incoherent scatter. The specimen reproducibility and sharpness of the peaks was found to be enhanced by hydrating with 5 mM EDTA. The effect of the irreproducibility was to increase the error in the determination of the limiting concentration of lipid at full hydration, $C_L$, which, in turn, propagated to large errors in the values in Table I. Values of $\bar{v}_w = 1$ g/mL and $\bar{v}_L = 0.97$ g/mL were used for all lipids. Lis et al. (1982) used $\bar{v}_L = 0.99$ g/mL for DOPC at 20 °C. This was temperature adjusted to 0.97 at 2 °C via the slope of ~0.01 g/mL per 10 °C found by Seddon et al. (1984) for several PEs. In any case, variation of $\bar{v}_L$ by 0.02 results in insignificant changes in the bilayer dimensions relative to the errors arising from the determination of $C_L$. For these reasons, the values in Table I should be considered more noteworthy for the general trend exhibited, which is always seen, than for the absolute values of the structural dimensions. We speculate that the odd behavior of these lipids at 2 °C is related to the very peculiar behavior of DOPE-Me at somewhat higher temperatures, as described under Results.

*X-ray Specimen Preparation.* Unless otherwise stated, all lipid specimen mixtures are specified in the text by weight fractions.

Lipids for the X-ray specimens were mixed to the proper ratio volumetrically from stock solutions in chloroform. The chloroform was then evaporated under nitrogen and the lipid resolubilized in cyclohexane. The cyclohexane solution was lyophilized directly in a glass X-ray capillary leaving about 5 mg of lipid. Early samples were prepared by drying the chloroform in the capillary under vacuum with no lyophilization. Lyophilization in cyclohexane was found to facilitate mixing of the lipid with dodecane and water and did not affect the phase behavior of the lipid. Dodecane was added to some samples, as specified in the text. The proper buffer was added, the sample was mixed mechanically, and the capillary was sealed. Samples in which the water concentration was critical were sealed before mixing. These were mixed by centrifuging the lipid back and forth, in the capillary, in a bench-top centrifuge, and then allowing the samples to equilibrate at the desired temperature for several days.

Unless otherwise stated, the aqueous solution consisted of distilled water. For the 15% egg-PC/18% soy-PE samples, the buffer used was 2 mM HEPES, 2 mM histidine, and 100 mM NaCl, pH 7.4, and for the specimen of Figure 5 the buffer consisted of 10 mM HEPES and 100 mM NaCl, pH 7.4. These buffers were used so as to be consistent with the protocols of earlier experiments. It was observed that the lamellar phases of DOPE-Me$_2$ were stable for long periods of time in a buffer consisting of 15 mM HEPES and 5 mM EDTA, pH 7.0. This buffer was used for the data of Figure 2a,c and for mixtures of DOPE-Me, lysolipid, and fatty acid. Distilled water, the buffer used for Figure 5, and the EDTA buffer yielded identical results for DOPE, DOPE-Me, and DOPC. In all cases, the aqueous solution was allowed to equilibrate for at least 2 h after mixing with the lipid. Prior to taking the X-ray diffraction data, samples were cycled in temperature between −30 and 85 °C at least once.

*Calorimetry.* Differential scanning calorimetry (DSC) specimens were prepared in much the same manner as the X-ray specimens. Distilled water (65% by weight) was added to about 5 mg of lipid in an aluminum pan. The pan was then sealed in a press. Data were taken on a Perkin-Elmer DSC-4 scanning calorimeter at a scanning rate of 40 °C/min.

*NMR.* $^{31}$P NMR spectra were obtained by using a Bruker WP-200 spectrometer operating at 81 MHz for $^{31}$P. Phospholipid mixtures (50 mg) were dispersed by vortex mixing in 0.8 mL of 2 mM HEPES, 2 mM histidine, and 100 mM NaCl, pH 7.4 at room temperature. Spectra were accumulated for up to 2000 transients employing a 15-$\mu$s 90° pulse, a 20-kHz sweep width, and a 1-s interpulse delay in the presence of broad-band proton decoupling. An exponential multiplication corresponding to 50-Hz line broadening was applied to the free induction decay prior to Fourier transformation.

## Results

*Lattice Dimensions.* The mesomorphic phase behavior and lattice basis lengths for DOPE, DOPE-Me, DOPE-Me$_2$, and DOPC above 0 °C in excess buffer are summarized in Figure 1 and Table I. The effect of successive methylation was to lower the chain melt transition temperature, $T_c$ (−5 to 10 °C for DOPE; −10 to −15 °C for DOPE-Me; and −15 to −20 °C for DOPE-Me$_2$ and DOPC), as determined by the disappearance of the sharp gel chain diffraction peak at roughly 4.2 Å, which is indicative of gel chains (data not shown). The $L_\alpha$ repeat distance increased upon methylation, with most of the increase occurring after the first methyl group had been added. For example, at 2 °C, the $L_\alpha$ repeats were 52, 61, 62, and 61 Å from DOPE to DOPC, respectively.

The $L_\alpha$ to $H_{II}$ transition temperature, $T_{BH}$, also increased upon methylation. For DOPE, $T_{BH}$ was 5–10 °C, consistent with earlier reports [see Tilcock and Cullis (1982) and references cited therein]. For DOPE-Me, a hexagonal phase was observed above roughly 65 °C, with peculiar behavior (to be described below). For DOPE-Me$_2$ and DOPC, the $L_\alpha$ phase extended to at least 85 °C, the highest temperatures examined in this study, consistent with the DSC results of Gagne et al. (1985). Again, note that a large change in $T_{BH}$ occurs after a single methylation. The $H_{II}$ basis length (center-to-center distance of adjacent cylinders), $d_H$, also increased upon methylation of DOPE. For example, at 65 °C, DOPE had a 67.0-Å basis, whereas DOPE-Me had a basis of 74.2 Å.

The basis length, $d_L$, of the fully hydrated $L_\alpha$ phase also increased with methylation. Recall that $d_L = d_W + d_B$, where

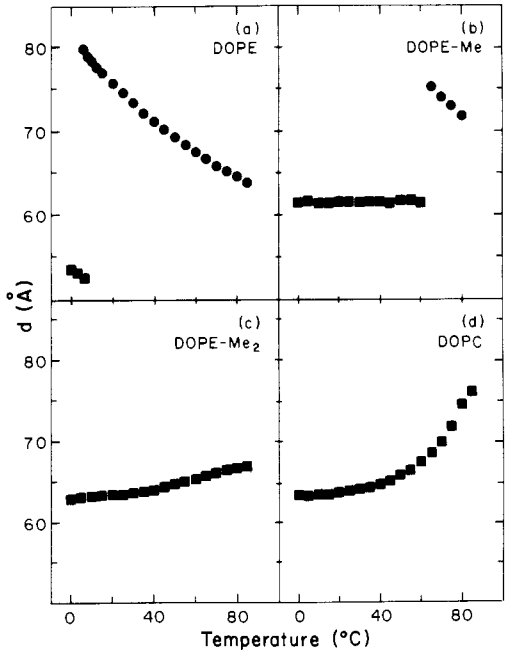


FIGURE 1: Phase and lattice basis vector lengths for DOPE through DOPC in excess water vs temperature. For $L_\alpha$ phases (■), the ordinate is $d_L$, while for $H_{II}$ phases (●), the ordinate is $d_H$. See Figure 8 for definitions of $d_L$ and $d_H$. For each specimen, the experimental protocol was to cool to −30 °C and then heat in 5 °C steps.

$d_W$ and $d_B$ are the interlamellar water and the bilayer thicknesses, respectively. It is of interest to determine how the change in $d_L$ partitions among changes in $d_W$ and $d_B$. For many zwitterionic lipids, the addition of water to dry lipid results in hydration and swelling of the lattice to the point where attractive and repulsive forces between the lamellae are in balance (Parsegian et al., 1979; Rand, 1981). Additional water will not be accepted by the lattice and pools as bulk water. The concentration above which water is in excess may be found by measuring $d_L$ vs the water concentration and determining the concentration above which $d_L$ no longer changes (Figure 2). Once the limiting water concentration is known, $d_B$ and $d_W$ may be determined by the procedure described under Materials and Methods.

The water thicknesses, $d_W$, as determined from the data of Figure 2, are shown in Table I. Note that $d_W$ increases upon methylation, indicating that the lattice affinity for water is enhanced upon methylation, with the largest increase accompanying the first additional methyl group. The static mean thickness of the water layers, $d_W$, may be modeled by the distance for which the hydration repulsion balances the van der Waals attraction (Rand, 1981). Following Lis et al. (1982), this balance of forces may be written

$$P_0 \exp(-d_W/\lambda) = F_{HYD} = [H/6\pi][d_W^{-3} - 2d_L^{-3} + (d_W + d_L)^{-3}] \quad (1)$$

where $d_B = d_L - d_W$. The term on the left represents the exponentially decaying hydration repulsion, where $\lambda$ is a decay length and $P_0$ represents the perturbation of water due to the lipid surface (Marcelja, 1976). The right-hand side of the equation is the van der Waals attraction of two lipid layers modeled as dielectric slabs, where $H$ is the Hamaker constant. Values for $F_{HYD}$ are given in Table I, where it is assumed that $H = 5.6 \times 10^{-14}$ erg [Lis et al., 1982; see also Evans and Metcalfe (1984), who obtain $H = 5.8 \times 10^{-14}$ erg for egg-PC]. A single methylation leads to a dramatic decrease in the magnitude of $F_{HYD}$ at equilibrium. Further methylation progressively decreases $F_{HYD}$ but with less dramatic changes.

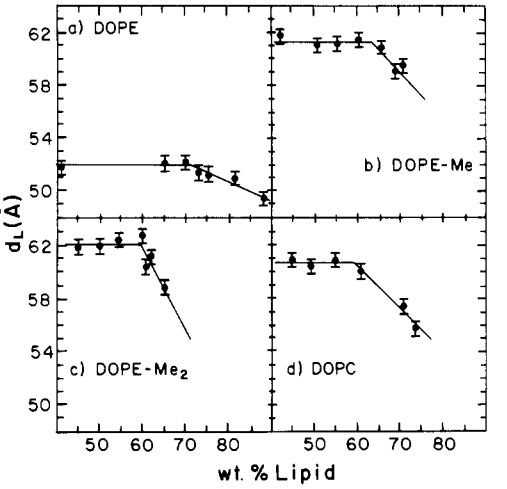


FIGURE 2: Lamellar basis vector length, $d_L$, vs the lipid concentration for DOPE through DOPC at 2 °C. The limiting water concentrations are listed in Table I.

It should be noted that whereas the qualitative trend in $F_{HYD}$ is well supported by the data, the actual numerical values are sensitive to uncertainties associated with the determinations of $d_W$ and $d_B$ (see Materials and Methods).

*Phase Behavior of DOPE-Me.* The X-ray apparatus used for this study was well suited for examination of phase transition dynamics on the time scale of minutes. Useful X-ray patterns could readily be obtained with less than a minute of X-ray exposure. Moreover, the specimen temperature could, under computer control, be rapidly slewed (~1 °C/s) and brought into thermal equilibrium in a minute or so. When pure $L_\alpha$ or $H_{II}$ phases were observed with DOPE and DOPC, the diffraction patterns settled within the 60-s time resolution of the instrumentation. When coexisting $L_\alpha$ and $H_{II}$ phases were observed with DOPE, the relative intensities of the $L_\alpha$ and $H_{II}$ diffraction peaks drifted slowly over many hours, indicating that the relative fraction of the lipid which was in one phase or the other was changing slowly. The coexisting $L_\alpha$ and $H_{II}$ peaks were sharp, and the background between the peaks was relatively low and flat. Sharp peaks indicate long-range order in the $H_{II}$ and $L_\alpha$ domains. The low, flat background indicates that most of the mass of the specimen was in the well-ordered lattices.

DOPE-Me, however, exhibited complex nonequilibrium behavior. A typical sequence of diffraction patterns is shown in Figure 3. The diffraction apparatus was programmed to step the temperature of a DOPE-Me speciment (30 wt % lipid in distilled water) from −30 to 75 °C and back to −30 °C in 5 °C steps. Each step consisted of a rapid adjustment of the temperature, followed by a 6-min equilibrium period and a 2-min X-ray exposure. The total cycle time per 5 °C step was 8 min. Selected exposures are shown in Figure 3. At low temperatures (Figure 3a), the specimen exhibited the lamellar pattern typical of gel-phase ($L_\beta$) lipid: a very strong first order, very weak second and third orders, and a moderately strong fourth order (off the edges of Figure 3a). Note the low level of incoherent X-ray intensity between the peaks (the level of zero X-ray exposure may be inferred from the dip near the center due to the beam-stop shadow). At higher temperatures the $L_\alpha$ phase pattern (Figure 3b–d), consisting of a monotonically decreasing sequence of intensities of the first four orders, became readily apparent. Note the rise in the background X-ray scatter and the progressive broadening of the high orders with increasing temperature. At 70 °C, a pattern indicative of a hexagonal lattice (peaks spaced in the ratio

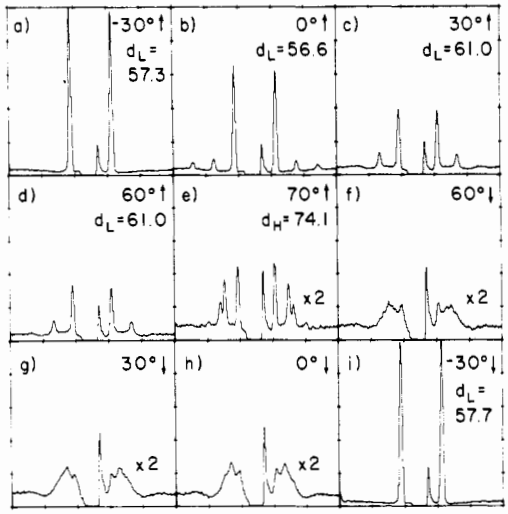


FIGURE 3: Azimuthal integrations (X-ray intensity vs scattering angle) for a sequence of diffraction patterns obtained from DOPE-Me. The experimental protocol, detailed under Results, was to stepwise vary the temperature from −30 to 75 to −30 °C in 5 °C steps. The lipid concentration was 30 wt % in distilled water. The dip near the center of each integration is due to the beam-stop shadow at a scattering angle of zero. The peak immediately to the right of the beam stop is from a wing of the main beam creeping around the edge of the beam stop. The arrows next to the temperature indicate if the temperature was on the heating (up arrow) or cooling (down arrow) part of the cycle. The lamellar ($d_L$) or hexagonal ($d_H$) basis vector lengths are indicated. All ordinates are to the same, arbitrary scale except (e–h), which are ×2. The intensities to the left and right of the beam stop are not symmetric because absorption and detector sensitivity uniformity corrections were not applied.

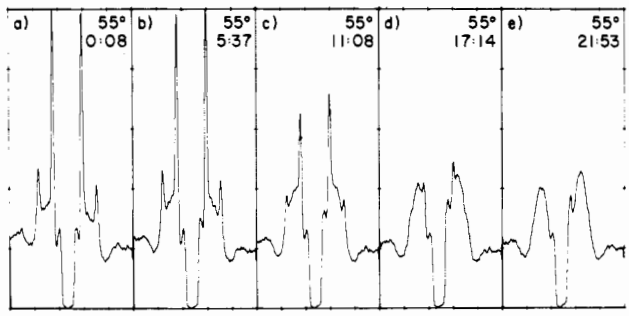


FIGURE 4: $L_\alpha$ diffraction patterns of DOPE-Me (30 wt % lipid in distilled water) obtained by heating from the gel phase are unstable on the time scale of hours at 55 °C. The elapsed time after the heating event (hours:minutes) is shown for each diffraction pattern. Note the gradual diminuation in intensity of the sharp lamellar peaks and the concomitant rise in broad scatter between the peaks.

1:√3:2:√7...) is seen. The actual temperature at which this first occurred was a function of the specimen water concentration and the equilibration time, but typically it occurred in the range of 60–75 °C. If one now reversed the temperature scan, the $L_\alpha$ phase pattern was replaced by a broad hump on top of copious incoherent scatter, indicative of a highly disordered specimen (Figure 3f). This disordered pattern continued until the chain freezing temperature, at which point the specimen adopted an $L_\beta$ phase pattern (Figure 3i) and the sequence could be repeated.

The $L_\alpha$ lattice of DOPE-Me was unstable at elevated temperatures, as may be seen in Figure 4. Here, a series of exposures were acquired over many hours while the specimen temperature was held constant at 55 °C. The lattice is seen to progressively disorder. The disordering was not due to lipid degradation because the system could be reset by deep cooling (see Figure 3). Note that the disorder in the diffraction occurs by a gradual rise in the diffuse intensity between the sharp

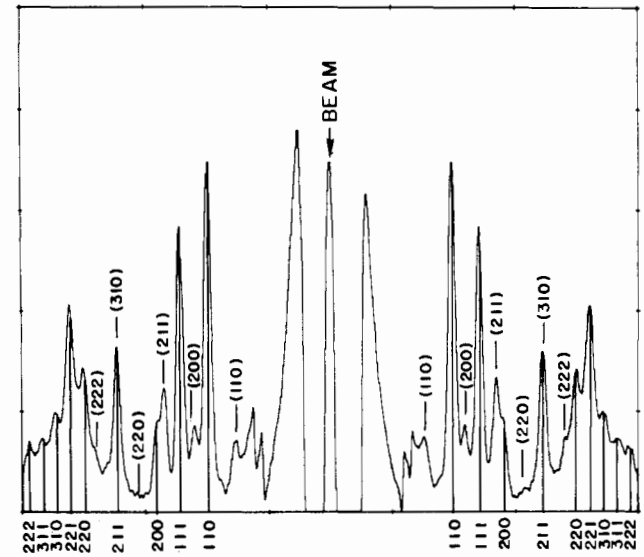


FIGURE 5: Disordered state of DOPE-Me (33 wt % lipid in buffer consisting of 15 mM HEPES and 100 mM NaCl, pH 7.4) obtained by cooling from the $H_{II}$ phase very slowly forms well organized cubic lattices. This specimen was sealed in an X-ray capillary and left at room temperature for 1.5 years; a densitometerization through an X-ray film exposure of the specimen is shown (specimen to film distance = 252 mm; exposure time = 69 h; temperature = 25 °C). The tick marks are the expected positions of the diffraction peaks from two cubic lattices that are indexed (*hkl*) near the tick. The indices without parentheses are consistent with either the *Pn*3*m* or *Pn*3 space groups. The indices enclosed in parentheses (indexed out to the 222 order) are for an *Im*3*m* space group. Note, however, that the orders observed for the second lattice do not unequivocally determine the space group. The features between the (110) orders are due to the X-ray camera. This specimen exhibited considerable incoherent scatter. In consequence, a constant was subtracted from the densitometer trace.

peaks, indicating that the fraction of the specimen which was well ordered decreased over time. The rise in incoherent scatter on short time scales seen in Figure 3 was the beginning of this disordering process. The disordering process proceeded slowly as temperature increased (Figure 3 and 4) but very rapidly if the specimen was cooled from the $H_{II}$ phase (Figure 3f).

The $H_{II}$ phase at 75 °C was stable for at least 3 days. No systematic effort was expended to find the lowest temperature at which the $H_{II}$ phase was stable.

The broad, disordered diffraction of Figures 3 and 4 evolved very slowly into well-defined lattices consistent with cubic symmetries. Figures 5 and 6 show the lattices that resulted when a sealed X-ray capillary was left undisturbed on the shelf at room temperature for 1.5 years. The peaks shown in Figure 5 index as two lattices, as seen in Figure 6. The specimen looked like a translucent gel with a slight gradation of translucence from the top of the capillary to the bottom. This resulted from a gradation of the relative fractions of the two lattices present, as was readily confirmed from diffraction patterns taken from the top and bottom of the capillary (data not shown).

As shown in Figure 6, one of the lattices consisted of nine orders of diffraction spaced in the ratio of √2:√3:√4:√6:√8:√9:√10:√11:√12. The smallest unit cell space groups consistent with orders spaced in these ratios are *Pn*3*m* and *Pn*3 with a 136-Å unit cell [see *International Tablets for X-ray Crystallography* (1968) for information on assigning space groups]. Three orders spaced in the ratio √1:√2:√3 were observed for the second lattice. A definitive lattice assignment on so few orders is not possible, although such spacings rule out either a single lamellar or a single hexgonal lattice as well as many of the cubic space groups. Of the

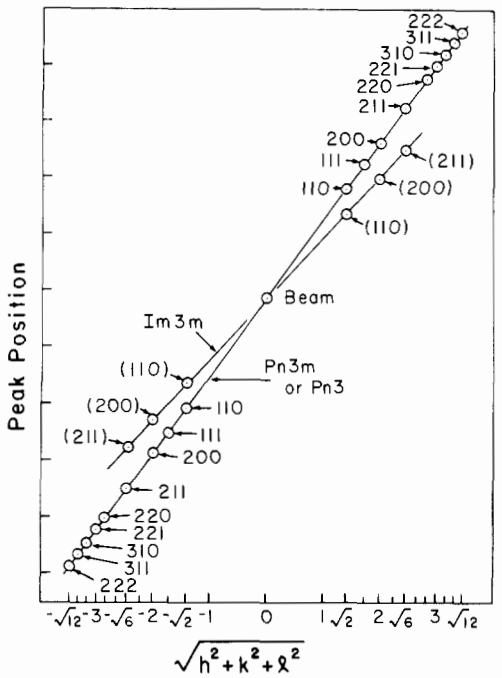


FIGURE 6: Scattering angles of the peaks of the two cubic lattices of Figure 5 vs $(h^2 + k^2 + l^2)^{1/2}$ for the *hkl* indices of the expected nonzero reflections. All points from each lattice should fall on a straight line whose slope is used to determine the dimensions of the unit cell.

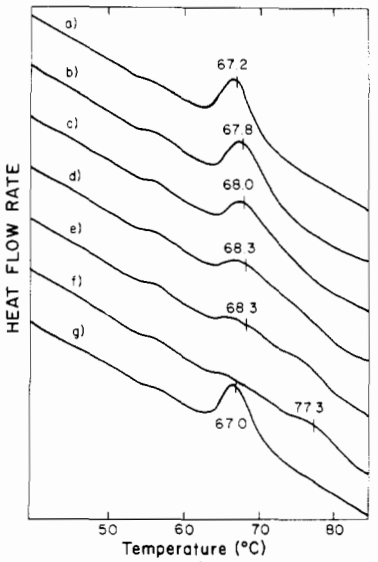


FIGURE 7: DSC traces for a DOPE-Me specimen (35 wt % in distilled water) show the nonequilibrium behavior of this lipid. The top trace resulted when the specimen was scanned from −40 to 85 °C at 40 °C/min. The temperature was then scanned at 40 °C/min to 20 °C and rescanned to 85 °C (trace b). This procedure was repeated for traces c–f. Note the gradual appearance of three peaks in trace f. The specimen was then cooled to −40 °C, thereby resetting the system, and the bottom trace (g) was run.

remaining space groups consistent with the diffraction, *Im3m* is mentioned specifically in light of the structures described under Discussion and by other authors (Charvolin, 1985; Luzzati et al., 1987). The body-centered lattice of the *Im3m* space group would have a unit cell of 175 Å.

Some lipid degradation may be expected after prolonged storage at room temperature. Specimens that had been stored up to 4 months were examined by gas chromatography and TLC and indicated that up to 2 mol % of the lipid had degraded. The effects of common lipid degradation products were examined by preparing fresh samples (overall water content of 60%) that were 98 mol % DOPE-Me and 2 mol % of either oleic acid, lysophospholipid (e.g., monooleic-PE and monooleic-PC in a 3:1 mol ratio to mimic monooleic-PE-Me), or oleic acid and lysophospholipid. These samples were rapidly cycled a few times between 25 and 70 °C and then allowed to remain at 25 °C. In all cases, diffraction consistent with the *Pn3m*/*Pn3* space groups could be seen immediately. Although the *Pn3m*/*Pn3* unit cell size varied between 125 and 140 Å, it is significant that at 80 °C all these specimens had a $H_{II}$ unit cell size within 0.5 Å of fresh, pure DOPE-Me. DOPE-Me stored for long periods at room termperature had similar unit cell sizes. These results indicate that DOPE-Me degradation products promote formation of cubic phases at 25 °C, and low fractions (<2 mol %) of such products have only a small effect on the $H_{II}$ phase unit cell size.

Differential scanning calorimetry thermograms characteristic of the nonequilibrium behavior of DOPE-Me are shown in Figure 7. Note the apparent hysteresis in the system.

The nonequilibrium behavior of DOPE-Me in excess water is summarized as follows:

(1) The system exhibits a peculiar thermal cycle. (a) Deep cooling into the gel ($L_\beta$) state resets the cycle. Several freeze–thaw cycles may be required to accomplish the reset. (b) Upon heating out of the gel phase, the system assumed a well-ordered $L_\alpha$ phase. Continued heating introduced an increasing fraction of disordered lipid. (c) Rapid continued heating induced a transition to a stable $H_{II}$ phase with a large basis vector. The apparent transition temperature of the transition is time and lipid concentration dependent. (d) Cooling out of the $H_{II}$ phase quickly disrupted the lattice structure. The $L_\alpha$ phase diffraction pattern observed on heating was replaced by broad, unsampled diffraction. Optically, the $L_\alpha$ phase was birefringent and readily coexisted with bulk water. The disordered state was optically isotropic and imbibed considerable water. The $^{31}P$ NMR of the disordered system exhibited an isotropic resonance [see, for example, Gagne et al. (1985)].

(2) Upon heating from the $L_\alpha$ phase, maintaining the system just below the apparent $L_\alpha$ to $H_{II}$ transition temperature slowly induces the disordered state on a time scale of days.

(3) The disordered state slowly converted to cubic lattices. The rate of conversion and the lattices seen were dependent on the water concentration, the degree of lipid degradation, and the thermal history.

*Connection to the Monolayer Spontaneous Curvature.* The slow, nonequilibrium behavior summarized above is by no means peculiar to DOPE-Me; rather, it appears to be a general feature of lipid systems with certain relative values of the spontaneous radius of monolayer curvature (Gruner, 1985). In this section the behavior of other lipid systems is described in support of this correlation. Prior to doing so, however, it is useful to summarize the literature relating to the spontaneous monolayer radius of curvature.

Lipid monolayers, which back-to-back form bilayers or roll into tubes that pack as $H_{II}$ phases, may be characterized by a spontaneous[2] (=intrinsic = equilibrium) radius of curvature, $R_0$, which represents the minimum elastic free energy state of the layer with respect to bend (Kirk et al., 1984; Gruner et al., 1985; Gruner, 1985). In general, in a quadratic ap-

[2] "Spontaneous", "equilibrium", and "intrinsic" radii are all equivalent names for the natural radius of curvature, $R_0$. From here on the term spontaneous radius will be used so as to be consistent with the bulk of the physics literature. Also, we sometimes speak in terms of the spontaneous radius of curvature, $R_0$, and sometimes in terms of it inverse, the spontaneous curvature, $1/R_0$.

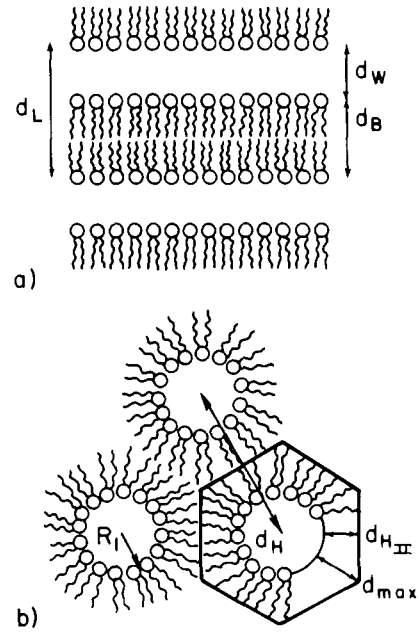


FIGURE 8: Schematics of $L_\alpha$ (a) and $H_{II}$ (b) phases. The average thickness of the hydrocarbon layer in the $H_{II}$ phase schematic is seen to vary between $d_{H_{II}}$ and $d_{max}$ with 6-fold symmetry as one rotates about a cylindrical water core.

proximation, a small deviation from $R_0$ for a layer of material changes the free energy per unit area by

$$\Delta F = \frac{K}{2}\left(\frac{1}{R_1} + \frac{1}{R_2} - \frac{1}{R_0}\right)^2 + \frac{K_G}{R_1 R_2} \qquad (2)$$

where $R_1$ and $R_2$ are the principal radii of curvature of the layer (Helfrich, 1973) and $K$ and $K_G$ are constants of the material. $R_0$ may be defined as the value that self-consistently minimizes eq 2 with respect to $R_1$ and $R_2$ for given values of $K$ and $K_G$. In general, $R_0$ is a function of temperature and decreases as temperature increases (Kirk & Gruner, 1985). In the $H_{II}$ phase, one principal radius of curvature may be taken as indefinitely large along the tube axis, in which case eq 2 reduces to

$$\Delta F = \frac{K}{2}\left(\frac{1}{R_1} - \frac{1}{R_0}\right)^2 \qquad (3)$$

It has been shown that $R_0$ characterizes the propensity for a lipid system to assume a nonbilayer configuration (Kirk et al., 1984; Kirk & Gruner, 1985; Gruner, 1985; Tate & Gruner, 1987). If $R_0$ is small, as for DOPE, then in the $L_\alpha$ phase $R_1 \simeq \infty$ and, by eq 3, a large drop in free energy may be accomplished by curling such that $R_1 \simeq R_0$; this typically drives the formation of $H_{II}$ phases. If $R_0$ is large, as for DOPC, then eq 3 says that the driving force is diminished. In addition, for large $R_0$, large positive hydrocarbon packing free energies must be considered in going into the $H_{II}$ phase (Figure 8; Kirk et al., 1984; Gruner, 1985). Thus, large $R_0$ values lead to stable $L_\alpha$ phases. Intermediate values of $R_0$, as will be shown to be the case for DOPE-Me, lead to the slow nonequilibrium behavior.

For many systems the addition of a small fraction of an alkane, such as dodecane, removes most of the opposing hydrocarbon packing energy and leads to low-temperature $H_{II}$ phases (Kirk & Gruner, 1985). It has been shown that, in certain cases, the size of the $H_{II}$ core in excess water may be taken as a good measure of $R_0$ (Gruner et al., 1986). $R_0$ is temperature dependent and decreases with increasing temperature. The decrease in $R_0$ with temperature accounts for

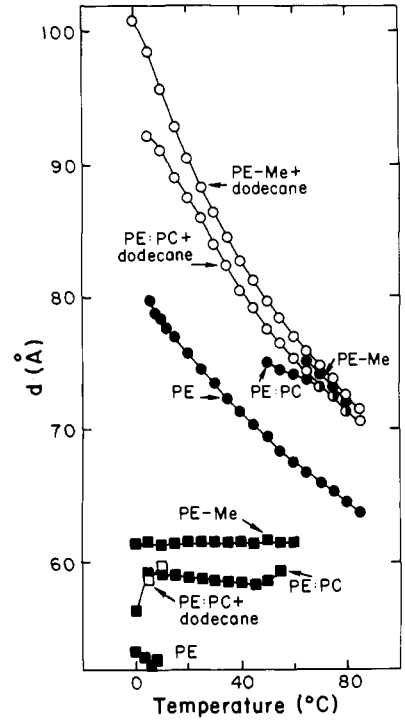


FIGURE 9: Lattice basis vector length vs temperature diagrams of several specimens. Squares represent $L_\alpha$ phases (ordinate = $d_L$), and circles represent $H_{II}$ phases (ordinate = $d_H$). Open symbols are for systems with dodecane (dry weights are ~95% lipid, ~5% dodecane). All specimens were in excess (~60 wt %) water. Data are shown for DOPE-Me, DOPE-Me + dodecane, DOPE/DOPC 3:1 (w/w); DOPE/DOPC 3:1 (w/w) + dodecane, and DOPE for comparison. As discussed in the text, the relative values of $d_H$ at a given temperature are related to the relative values of $R_0$, with larger $d_H$ values corresponding to larger $R_0$ values.

most of the decrease in $d_H$ in Figures 1 and 9.

Adding dodecane to a DOPE-Me specimen (37.6% DOPE-Me, 2.4% dodecane, 60% distilled water by weight) induced a low-temperature $H_{II}$ phase, as shown in Figure 9. Also shown for comparison are the $H_{II}$ dimensions of DOPE in excess buffer and the DOPE-Me $H_{II}$ phase in the absence of dodecane. Note the larger values of $d_H$ for the DOPE-Me $H_{II}$ phase relative to DOPE, indicative of larger values of $R_0$. Such relatively large $R_0$ values are termed "intermediate" values because they characterize specimens intermediate between those that readily adopt $H_{II}$ phases ($R_0$ small, such as in DOPE) and those that are normally in the $L_\alpha$ phase ($R_0$ large, such as in DOPC).

Intermediate $R_0$ values may also be obtained by mixing small and large $R_0$ lipids. Insofar as the lipids remain intimately mixed, the $R_0$ value of the mixture, being a colligative property of the system, is a compromise among the values of the constituents. Figure 9 shows the dimensions of a DOPE/DOPC 3:1 (w/w) system in excess buffer superimposed on that of DOPE-Me. The DOPE/DOPC ratio was chosen by trial and error to cause the $d_H$ vs $T$ curve of Figure 9 to be similar to that of DOPE-Me. Although the exact dependence of $R_0$ vs $T$ varies with the lipid head group and chain (S. M. Gruner, unpublished results), DOPE-Me and a DOPE/DOPC ratio of 3:1 are similar enough to one another that good overlap of $d_H$ vs $T$ is seen for the pure $H_{II}$ phases. Below 65 °C, the slope of both the $L_\alpha$ and $H_{II}$ repeat spacings change abruptly in the DOPE/DOPC 3:1 specimen without dodecane. Similar behavior seen with other mixed lipid systems has been interpreted as different ratios of the two lipid species (demixing) in the $L_\alpha$ and $H_{II}$ phases (Tate & Gruner, 1987). The similarity of DOPE/DOPC mixtures to DOPE-

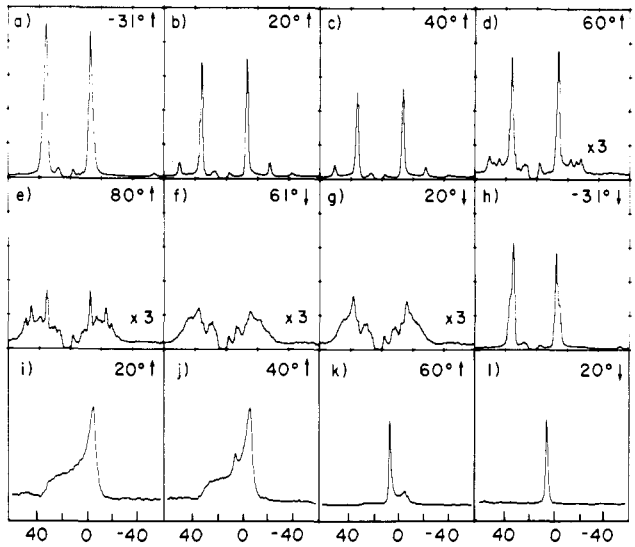


FIGURE 10: Selected radial integrations of the diffracted X-ray intensity (a–h) are shown for a 85 dry wt % soy-PE, 15 dry wt %, egg-PC specimen (~60% distilled water) as the temperature is stepped from −30 to 80 °C in 10° steps. Note the similarity in behavior to DOPE-Me (Figure 3). Selected $^{31}P$ NMR traces for a similarly cycled specimen are shown in (i–l). The rise in disorder in the X-ray diffraction shows up as an isotropic peak in the NMR. The abcissas for the NMR data (i–l) are in parts per million frequency shift from a freely tumbling phosphate.

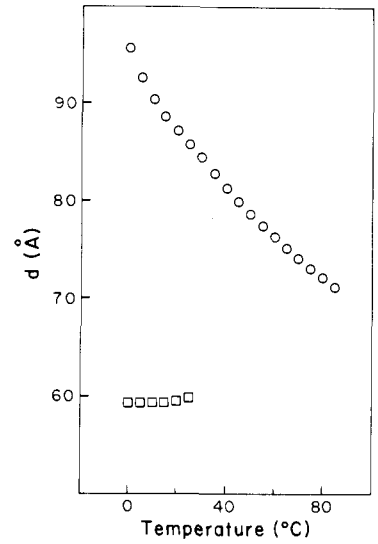


FIGURE 11: Lattice basis vector lengths vs temperature for soy-PE egg-PC = 85:15 that has been mixed to 5 wt % with dodecane and diluted with 60 wt % buffer (see Materials and Methods). Refer to Figure 10 for an explanation of the symbols. Note the large $d_H$ values for the soy-PE/egg-PC mixture, corresponding to intermediate $R_0$ values.

Me was pointed out by Kirk (1984) and more recently by Ellens et al. (1986). Note that at a ratio of 3:1 DOPE/DOPC the system has very roughly the same average number of methyl groups per molecule on the quaternary nitrogen as DOPE-Me. The peculiar thermal cycle behavior of DOPE-Me is also present with the DOPE/DOPC mixture but in a less pronounced manner (data not shown). It is possible that this system may demix in the $L_\alpha$–$H_{II}$ transition zone, an avenue of behavior that, obviously, is not possible in pure DOPE-Me water dispersions.

Nonequilibrium phase behavior strikingly similar to DOPE-Me is readily observed in other systems. For example, Figure 10 shows the behavior of a mixture of 85% soy-PE and 15% egg-PC dispersed in buffer (see Materials and Methods) to a water weight fraction of 60%. Upon addition of dodecane (5% of total nonwater weight; Figure 11), the system is seen to have intermediate $R_0$ values relative to soy-PE (data not shown). Soy-PE, by contrast, behaves much like DOPE.

## Discussion

Methylation of the DOPE nitrogen has potent effects on both the phase behavior of the lipid and the structural dimensions of the resulting phases. For example, a single methylation of DOPE causes large changes in the thickness of the interlamellar water (Table I) and a large shift of $T_{BH}$ to higher temperatures. Similar results were found by Fuller et al. (1983) for methylated egg-PE and, more recently by the same group, for methylated transesterified egg-PE [V. A. Parsegian and R. P. Rand, private communication; see also Sen et al. (1986)]. The challenge is to understand how methylation causes these changes.

Methylation of the nitrogen has several direct effects. It replaces a hydrogen-bonding proton; it alters the affinity of the nitrogen for the other hydrogens in the quaternary nitrogen group, thereby affecting the dipole moment of the head group; and it sterically interferes with the approach of the nitrogen group to adjacent head groups. Understanding the consequent effects on a liquid of head groups constrained to be oriented on a plane would, indeed, be difficult. The problem is further complicated by interactions with water on one side and with the volume requirements of the chains on the other. A molecular dynamics calculation of the appropriate magnitude is probably beyond current capabilities, even if the interactions between neighboring molecules were understood. Consequently, one adopts the alternative approach of identifying phenomenological forces that relate directly to the observed structural dimensions of the phases and attempts to at least understand qualitatively how methylation affects the phenomenological forces.

*Structure of the $L_\alpha$ Phase.* Consider, for example, the width, $d_w$, of the interlamellar water. In the most widely accepted picture (Rand, 1981), the static equilibrium value of $d_w$ is the width for which the fundamentally understood van der Waals attraction (the right-hand side of eq 1) counterbalances the poorly understood phenomenological force known as hydration repulsion (the left-hand side of eq 1). Assuming that the Hamaker constant for PE is similar to that for PC, then the rightmost column of Table I indicates that the effect of putting a methyl onto DOPE is to increase the effective net repulsion, thereby pushing the bilayers further apart and increasing the equilibrium water width. In the Marcelja (1976) description, increased repulsion correlates with increased perturbation of the water adjacent to the lipid surface. A plausible, although speculative, scenario is that a competition exists between water and the nitrogen group with respect to hydrogen binding to the phosphates of other lipid molecules. The distance between the nitrogen and phosphorus atoms of a head group is large relative to the size of a water molecule. In consequence, water molecules immediately adjacent to either of these atoms feel very strong electrostatic forces. Insofar as a hydrogen bond mediated association of the intermolecular nitrogen and phosphate groups is present much of the time, then on the length scale of a water molecule the associated groups are more electroneutral and may be less prone to hydrogen bond to water. This releases constraints on the affinity and orientation of adjacent waters. Moreover, the intermolecular association between head groups may resist increases in the area per molecule more effectively than if water molecules, with their added degrees of orientational freedom, mediate the association.

Intermolecular hydrogen bonding between the non-ester phosphate oxygens and the quaternary nitrogen groups of adjacent lipid molecules has been suggested as crucial to the differences between PE and PC [for reviews, see Boggs (1984) and Brown et al. (1986); see also Sen and Hui (1986)]. Such a linkage between adjacent head groups is clearly evident in the crystal structure of DLPE (Hauser et al., 1981). Linkage also exists in crystalline PCs but is mediated by included water atoms. The reader is referred to sections III C-2 and III C-3 of Hauser et al. (1981) for an excellent discussion of these linkages. In both crystalline and liquid-crystalline PEs and PCs, the predominant orientation of the intramolecular line joining the phosphate and nitrogen is thought to be mostly parallel to the membrane plane, making such linkages stereochemically possible [see Hauser et al. (1981) and references cited therein]. Our point is simply that the in-plane hydrogen-bonding interactions couple to the out-of-plane interactions via the adjacent water molecules. Clearly, much work remains to be done to turn these speculations into a quantitative picture of the interactions present.

*Effect of Methylation on the Phase Behavior.* The effect of methylation on the lamellar to nonlamellar phase behavior can be understood in phenomenological terms by invoking effects upon the spontaneous curvature of the lipid monolayers (see Connection to the Monolayer Spontaneous Curvature under Results). We assume that the sum total of the effects that have often been considered as contributing to an "intrinsic molecular shape" results in a desired monolayer curvature. The utility of speaking of a spontaneous curvature is that it combines a large number of complicated microscopic contributions into a more readily measured set of phenomenological quantities (see below). Moreover, at least for small deviations from the spontaneous curvature, the energy of bending the layer can be written in the simple quadratic approximation of eq 2.

The concept of an intrinsic molecular shape giving rise to a monolayer curvature is not new, dating back at least to Tartar (1955) [see Rilfors et al. (1984) for a review]. The use of an intrinsic molecular shape presents difficulties in that one usually refers not to a hard-core molecular shape but, rather, to the shape of the average volume per molecule that minimizes the free energy of the system. Many energetic factors contribute to this volume, including hard-core, van der Waals, hydrogen-bond, electrostatic, rotational isomeric, and other energies. Furthermore, it is often unclear how the free energy changes with alterations of the available molecular volume. By contrast, the fundamental parameters of a spontaneous curvature description, i.e., $K$ and $R_0$ of eq 3, have been measured (Gruner et al., 1986).

Helfrich and co-workers [see, for example, Helfrich (1973) and Deuling and Helfrich (1976)] have used the notion of a spontaneous curvature to explain the shapes of vesicles and cells. They pointed out that naturally occurring bilayers may have monolayer asymmetry and that this may lead to a spontaneous tendency for the bilayers to curve with a free energy density, for small deviations, given by eq 2 (with $K$, $K_G$, and $R_0$ referring to bilayer parameters). Kirk et al. (1984) used a spontaneous *monolayer* curvature to explain mesomorphic transitions, such as the $L_\alpha$–$H_{II}$ transition, in which the shape of the monolayer abruptly changes. Specifically, it was assumed that lipid monolayers of a given composition in excess water can minimize a bending free energy by curving toward a spontaneous radius of curvature, $R_0$. Equation 3, with $K$ and $R_0$ now referring to monolayer properties, also generally describes the surface energy density of small deviations of monolayer curvature, $1/R$, from the spontaneous curvature, $1/R_0$.

Kirk et al. (1984) assumed that $R_0$ is a characteristic of the lipid system at a given temperature and is a well-defined number even for monolayers that are strongly bent. Then for cylinders or planes, for which $R_2 \simeq \infty$, eq 2 reduces to eq 3. (Note that this assumes a quadratic approximation. If, in fact, $R_1 \simeq R_0$ in the $H_{II}$ phase, as discussed below, then eq 3 may only be a limited approximation of the energy required to fully flatten the monolayers.) The potentials postulated by Israelachvili and co-workers can also be reduced to a similar form [e.g., see Israelachvili et al. (1980) for a review and Kirk et al. (1984) for a discussion]. The formation of mesophases with curved monolayers are then driven by the tendency of the layers to curve toward, or express, their spontaneous curvature.

Kirk et al. (1984) also noted that energies other than that due to spontaneous curvature (eq 3) are required to understand mesomorphic transitions, such as $L_\alpha$–$H_{II}$, for which the monolayer curvature changes discontinuously. These other energies are required since $R_0$ is assumed to be a characteristic of the monolayer, not the specific phase. If one assumes that the monolayers of $H_{II}$ phases curl into cylinders such that $R_1$ approaches $R_0$ so as to minimize the right-hand side of eq 3, then competing free energies act to force $R_1$ away from $R_0$ in the $H_{II}$ to $L_\alpha$ transition. For electrically neutral, polar lipids in the presence of sufficient water, Kirk et al. (1984) identified the predominant competing free energy as that associated with the packing of hydrocarbon chains. One assumes that each local geometry is associated with an optimum chain length and that deviations from this length cost a free energy of stretching or compressing the chains. In the $L_\alpha$ phase, the chains are all at the same average length, and this contribution is small. However, in the $H_{II}$ phase, there is a systematic variation in chain length around the $H_{II}$ tube (Figure 8) that raises the free energy of this geometry. Thus, if $R_0$ is "small", as discussed below, then in the $L_\alpha$ phase $R_1 \sim \infty$, so $(1/R_1 - 1/R_0)^2 \simeq (1/R_0)^2$, and the curvature energy of eq 3 is high. The chain packing energy is low. In the $H_{II}$ phase for which $R_1 \sim R_0$, the curvature energy is low but the chain packing energy is high. Since the predominant phase behavior is governed primarily by the *sum* of the curvature and chain packing energies, it is possible for either the $L_\alpha$ or $H_{II}$ phases to have an overall lower free energy. In Kirk (1984) and Kirk et al. (1984) it is shown how this can arise in the limited water case (i.e., the lyotropic transition). The argument in Gruner (1985) shows how this may also arise in the case of excess water (i.e., the thermotropic transition).

Considerable experimental evidence has been gathered in support of the curvature vs hydrocarbon packing model. Kirk (1984) and Kirk and Gruner (1985) demonstrated that a few weight percent of dodecane or tetradecane, which might be expected to relieve hydrocarbon packing constraints, readily induced $H_{II}$ phases. Certain hydrophobic polymers also promoted the formation of $H_{II}$ phases (Gruner, 1985). These results were explained by assuming that the expression of curvature in the $H_{II}$ phase was constrained by chain stretching. Gruner et al. (1986) measured the work of changing the radius of $H_{II}$ cylinders via osmotic methods. It was found that the change in work followed eq 3 over a surprisingly wide range, where $R_1$ was taken as the water tube radius. It was also found that the value of $K$ that was determined was plausible in view of measurements done on bending bilayers [see Gruner et al. (1986) for references]. Significantly, the values of $R_0$ that best fit the data were very close to the radius of the $H_{II}$ water cores obtained with excess water. The importance of this last

result is twofold: *First, it suggests that, in excess water, $R_0$ largely determined the radius of the $H_{II}$ tubes.* Second, it suggests that, at least in the cases examined, the "water tube" radius determined by the Luzzati method (Luzzati, 1968) defines a surface about which eq 3 is approximately valid, i.e., that eq 3 applies to a surface near the lipid head groups. Finally, Tate and Gruner (1987) showed that chain packing stress can also be relieved by the addition of a small amount of long-chain lipid to a system of otherwise similar chains.

The literature reviewed, above, may be summarized as follows:

(1) At a given temperature, in the presence of sufficient water and in the absence of other constraints (e.g., hydrocarbon packing constraints), lipid monolayers of a given composition have a spontaneous tendency to curve to a radius $R_0$.

(2) $R_0$ is defined to a surface near the lipid head groups. [Specifically, this is the case for DOPE and DOPE–DOPC mixtures [see Gruner et al. (1986)]. It is not known if this is generally true for other lipid systems.]

(3) Hydrocarbon packing constraints compete effectively with the spontaneous curvature in determining the mesomorphic behavior. In many systems, small fractions (5–20% of the nonwater weight) of added alkanes, such as dodecane or tetradecane, can remove most of this competition without strongly altering the spontaneous curvature.

(4) *In comparing similar lipids, such as the methylated analogues of DOPE, the relative magnitudes of $R_0$[3] are measures of the driving forces toward curvature and are, therefore, quantitative measures of the relative mesomorphic tendencies of the lipid systems.*

The four points summarized in the preceding paragraphs facilitate the practical use of the spontaneous radius of curvature, $R_0$, as a quantitative measure of phase behavior. Referring to Figure 8, note that

$$d_H = 2(R_1 + d_{H_{II}})$$

But, by point 2 of the preceding paragraph, $R_1 \simeq R_0$ at full hydration; consequently

$$R_0 \simeq d_H/2 - d_{H_{II}} \quad (4)$$

The practical value of eq 4 is that for many systems of biological interest $d_H$ varies by tens of angstroms with temperature, while $d_{H_{II}}$ falls within a much narrower range [see, for example, Luzzati and Husson (1962) and Kirk and Gruner (1985)]. Moreover, $d_H$ is readily determined by X-ray diffraction, allowing an easy determination of an approximate value of $R_0$ for $H_{II}$ systems. Many systems that are not normally $H_{II}$ at the desired temperature can be induced to assume the $H_{II}$ phase by the addition of 5–20% dodecane or tetradecane (point 3, above), thereby extending the practical range of eq 4. For example, the values of $d_H$ at 70 °C in Figures 1 and 9 show that DOPE has a smaller $R_0$ than DOPE-Me over the temperature range examined, and Figure 9 shows that addition of 5 wt % dodecane has very little effect on the spontaneous radius of curvature of DOPE-Me.

*Phase Behavior as a Function of $R_0$.* Comparison of DOPE and DOPE-Me (parts a and b of Figure 1) at an arbitrary temperature in the $H_{II}$ phase, say at 70 °C, indicates that a single methylation has resulted in an increase of the $H_{II}$ basis length by about 8 Å. In view of the discussion about eq 4, above, this difference reflects an increase in the spontaneous radius of curvature of about 4 Å and a comparable increase in the radius of the $H_{II}$ water cores. As discussed in Gruner (1985), an increase in the radius of the water core requires that the hydrocarbon chains must stretch to different lenghts to fill the hydrocarbon zone, thereby incurring a considerable cost in free energy. (A simple way of visualizing this is to picture a limiting case of Figure 8 for which $R_1 \gg d_{H_{II}}$; in this case, the distance $d_{max}$ can be made to exceed even the fully stretched length of a hydrocarbon tail.) Assuming that the predominant monolayer shape is given by that geometry which minimizes the *sum* of the curvature and hydrocarbon packing energies, one asks if there exist geometries for which this sum is less than for those shown in Figure 8.

Global minimization of geometry-dependent free energies over the space of all possible monolayer geometries is a very difficult mathematical problem. However, as pointed out in Kirk et al. (1984), comparisons between specific geometries can be made in cases where integrations of the free energy functionals are explicitly tractable. More simply, scaling arguments can be applied to geometries consistent with the observed diffraction patterns. For example, an $H_{II}$ geometry alternative to that shown in Figure 8 is one in which the lipid tubes form perfect hexagons with uniform monolayer thickness, $d_M$, and hexagonal water cores. Relevant length scales include $R_0$, assumed to be defined to a surface near the head groups, $d_M$, and atomic dimensions. In the limit as $R_0 \rightarrow 0$ atomic roughness of the head groups renders energy distinctions between cylindrical and hexagonal water cores meaningless, and this case merges with the cylinder case shown in Figure 8. Here, both constant $R_0$ and constant monolayer thickness can be universally satisfied, suggesting that the $H_{II}$ phase is a global (but not necessarily unique) minimum for very small $R_0$. We suggest this explains the prevalence of $H_{II}$ phases when $R_0$ is very small, i.e., at the high-temperature end of the phase diagrams. When $R_0 \rightarrow \infty$, $L_\alpha$ phases can again satisfy both a constant desired curvature ($R_0 \simeq \infty$) and a constant monolayer thickness over the whole surface. Thus, for large $R_0$ lipid systems, bilayers probably represent global minima.

Intermediate $R_0$ values are more problematic. As $R_0$ grows from a very small value, a water core intermediate between a perfect circle and a hexagon is a compromise between curvature and chain stretch energies. We know of no experimental study that has examined the detailed shape of large $H_{II}$ cores and, therefore, cannot exclude the possibility of noncylindrical cores.

The data presented under Results, above, clearly demonstrate that specimens which are at least 98% DOPE-Me form lattices with cubic symmetries (Figures 5 and 6). Note that these cubics appear *in between* $L_\alpha$ and $H_{II}$ phases. This position for cubic phases in the phase diagrams of dual-chain lipids has been noted by many groups [see, for instance, Larsson et al. (1980), Hui et al. (1981, 1983), Wieslander et al. (1981a), Gutman et al. (1983), Seddon et al. (1984), Rilfors et al. (1984, 1986), Brentel et al. (1985), Charvolin (1985),

[3] The words "relative magnitudes of $R_0$" are used to remind the reader that the $R_0$ values of diverse lipid systems should not, in general, be directly compared. If the systems had comparable monolayer rigidities, $K$, and comparable monolayer thicknesses and took comparable energy to stretch the chains a given length, then it would be reasonable to do an absolute comparison. However, too little is known about these elastic properties for monolayers of diverse compositions to compare the absolute value of $R_0$ for arbitrary systems. Thus, we would expect, if $H_{II}$ phases are obtainable, the $d_H$ vs $T$ curve of, say, diarachinoyl-PE (DAPE, which has saturated chains 20 carbons long) to fall below that of DAPE-Me and DAPE to exhibit more of a tendency to go into the $H_{II}$ phase than DAPE-Me. However, until more is understood about the microscopic interactions in lipids, one should be reluctant to directly compare the $d_H$ vs $T$ curves of, say DOPE and DAPE. Note, however, that DOPE-Me and DOPE:DOPC (Figure 9) both have similar $T_{BH}$ (~60 °C) and similar values of $d_H$.

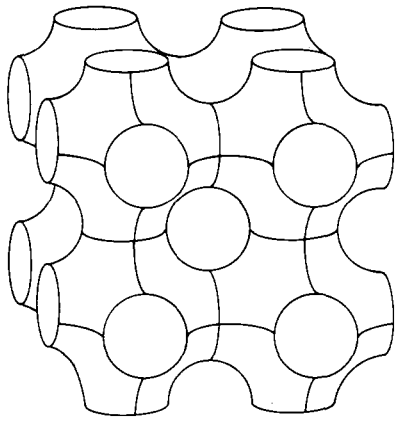

FIGURE 12: Schematic of several repeating units of a periodic minimal surface (PMS). If the surface is draped on either side with lipid monolayers such that the terminal chain methyls of the monolayers touch on the surface, then the resulting structure is a cubic lattice with an *Im3m* space group. This surface is variously known as Schwartz's surface, the S surface, or the Plumber's nightmare.

Eriksson et al. (1985), Lindblom et al. (1986), Siegel (1986d), and Luzzati et al. (1987)]. In excess water, the decrease in $d_H$ with increasing temperature (e.g., Figure 1a) is attributed to a decrease in $R_0$ (Kirk & Gruner, 1985; Gruner et al., 1986). The cubic lattices of DOPE-Me are associated with values of $R_0$ *intermediate* to those clearly associated with $L_\alpha$ and $H_{II}$ phases. On the basis of the available diffracted orders, space groups consistent with *Pn3m*/*Pn3* and *Im3m*, etc., have been observed in the DOPE-Me–water system (see Results). Therefore, one seeks cubic monolayer geometries with these space groups and for which the sum of the curvature and hydrocarbon packing energies is lower than for $L_\alpha$ or $H_{II}$ phases *only* if $R_0$ is not very large or very small.

Likely candidate surfaces are related to the periodic minimal surfaces (PMS). See Figure 12 and Hyde and Andersson (1985) and Schoen (1970) for models of, and references to, PMS. The surfaces of concern are periodic in three dimensions, display the correct cubic space groups, and have the property that every point on them is a saddle point such that $1/R_1 + 1/R_2 = 0$, i.e., have zero net curvature everywhere. An example of such a surface with space group *Im3m*, when draped with monolayers, is shown in Figure 12. Another, more complicated surface, when draped with monolayers, has the space group *Pn3m*. One imagines draping a monolayer on either side of this surface such that the PMS surface is at the chain terminal methyl midplane of a complex, multiply connected bilayer. The surface is macroscopically continuous in that lipid molecules can diffuse over many unit cells and over macroscopic distances without leaving a monolayer. Yet the two locally opposed monolayers on either side of the minimal surface are distinct: no route of diffusion continuously within a monolayer can bring the head groups of one monolayer in contact with head groups of the opposed monolayer. The bilayer divides the water volume into two, mutually congruent, interpenetrating, macroscopically continuous, but distinct, water channel networks. Recently, considerable attention has been focused on PMS as a model for lipid cubic phases [e.g., see Hyde et al. (1984), Charvolin (1985), Brentel et al. (1985), Mackay, (1985) Larsson and Andersson (1986), Rilfors et al. (1986), and Luzzati et al. (1987) for references and discussion].

Evidence is accumulating to suggest that most, if not all, inverted binary lipid–water cubic structures are bicontinuous (Rilfors et al., 1986). Earlier proposed cubic structures consisting of close-packed, discrete, reversed (water-cored) spherical micelles are, in most cases, inconsistent with NMR measurements of macroscopic lipid diffusion (Charvolin, 1985; Rilfors et al., 1986). Kirk et al. (1984) predicted, on the basis of curvature vs hydrocarbon packing arguments, that reversed spherical micelle cubic structures in binary systems would be energetically unfavorable.

A surface of zero net curvature seems, at first glance, inconsistent with the observed position of the DOPE-Me cubics between $L_\alpha$ and $H_{II}$ phases, i.e., at positions of intermediate values of curvature, $1/R_0$. Recall, however, that the appropriate surface within the depth of the monolayer to which $R_0$ is defined is not at the terminal hydrocarbon methyls but near the head groups (Gruner et al., 1986). Thus, if the terminal hydrocarbon methyls drape a surface of zero net curvature, the two surfaces appropriate to a curvature energy calculation are on either side of the zero curvature surface and are removed from it by the thickness of the hydrocarbon chain layer. These two head-group surfaces do not, in general, have zero net curvature. In fact, the head-group surfaces are very near the surfaces of mean *constant* curvature recently examined by Anderson (1986). Moreover, the surfaces that are a uniform distance, $d_M$ (i.e., a hydrocarbon chain thickness) off the minimal surface and the surface of constant mean curvature, $1/R_0$, are progressively less congruent as the ratio $d_M/R_0$ increases. In other words, only for values of $R_0$ that are not too small, in units of $d_M$, can the head groups have near constant curvature, $1/R_1 + 1/R_2 \simeq 1/R_0$, and still have near constant hydrocarbon thickness. Leibler (private communication) and Charvolin (1985) independently arrived at similar conclusions. Explicit calculations of the competition between model curvature and hydrocarbon packing effects have recently shown that there exists a range of parameters over which PMS cubic geometries should be favored over $L_\alpha$ and $H_{II}$ geometries (Anderson et al., 1988).

*Kinetics of the Cubic Phase Transition.* Figures 3, 5, and 10 illustrate the difficulties of determining the stable equilibrium phase diagrams of intermediate $R_0$ systems. How does one recognize stable phases when nonequilibrium lamellar states persist for very long times or when transient, but slow, disorganized structures mask the underlying stable geometry (e.g., Figures 4e)? There is, of course, no simple answer to this question. But an appreciation of the phenomenology of intermediate $R_0$ systems provides the investigator with valuable clues which indicate that the system may not necessarily be in stable equilibrium. This phenomenology is summarized at the end of Phase Behavior of DOPE-Me.

To illustrate the problem, consider the following simple question: What is the phase sequence and transition temperature of DOPE-Me in excess water? In a careful study of DOPE-Me, Gagne et al. (1985) noted that reproducible behavior required starting from a common state ($L_\alpha$); hence, they took care to preincubate their samples at 0–2 °C for 24 h. Their DSC showed only a broad shallow peak at 73 °C. $^{31}P$ NMR indicated an initial lamellar line shape that gave rise to a growing isotropic resonance above ~30 °C. At 60 °C only the isotropic resonance was apparent, while at ≳70 °C an underlying hexagonal phase line shape was seen. Freeze-fracture indicated bilayer vesicles with "occasional ridges and furrows" at 4 °C and increasingly complex lipid structures at 25 and 50 °C, including "small clusters of $H_{II}$ cylinders" at 50 °C. Cubic phases were not identified. Given this complicated sequence, it is difficult, as in our study, to say within a few degrees where $L_\alpha$ ends, where $H_{II}$ starts, and what is in between. It is also of interest to compare the DSC thermograms of Gagne et al. (1985) to our thermograms

(Figure 7). We believe the apparent differences are due to the heating rates (slow in their case, rapid in ours) and the overall water concentration (<1% lipid in their case; the specimen in Figure 7 was 65% water, which is still fully hydrated in the usual sense of being beyond the $L_\alpha$ or $H_{II}$ swelling limits). The behavior of DOPE-Me is dependent on the specimen history, the water concentration, even above "excess", and the rate of change of temperature. Unless one is very careful, the interpretation will vary with the time scale and the probe being utilized.

Ellens et al. (1986), in a study of the interactions of DOPE-Me liposomes, also noted the difficulties in determining the transition temperatures of the DOPE-Me phases. They recognized the necessity of resetting the system to a common state by deep cooling and commented on the connection between cubics and the isotropic $^{31}P$ NMR resonance noted earlier by Rilfors et al. (1984). Ellens et al. (1986) initiated events by preparing DOPE-Me liposomes at pH 9.5 and inducing aggregation by rapidly dropping the pH to 4.5. Since the behavior of DOPE-Me is independent on the specimen history, it is possible that the initial DOPE-Me states obtained by pH-collapsing liposomes will differ from those obtained from temperature changes of concentrated $L_\alpha$ phases. A detailed comparison of these two routes of changing the state of DOPE-Me has yet to be performed.

The results reported here demonstrate that lipid degradation products affect the kinetics of the cubic phases seen with DOPE-Me. This does not necessarily mean that distinct cubic phases do not occur in the pure DOPE-Me/water system. For instance, suppose that a room temperature free energy minimum associated with pure DOPE-Me and water is surrounded by sufficiently high activation energy walls that months are required for the transition to come into equilibrium. Suppose, further, that lipid degradation products act primarily to lower the activation barrier of the preexisting minimum associated with the cubic phase. Because lipid degradation products are generated on a time scale comparable to the equilibration time of the cubic phase, this case cannot readily be distinguished from the case of the degradation products creating a new free energy minimum corresponding to a cubic phase.

Several features of the behavior of DOPE-Me suggest, but do not prove, that the pure lipid has cubic phases with very slow equilibration times and that the degradation products primarily act to speed up equilibration. First, DOPE-Me disorders rapidly when cooling out of the $H_{II}$ phase but before lipid degradation has occurred. If a lamellar phase were the true equilibrium phase, why is a lamellar phase not formed upon continued incubation below the $H_{II}$ phase temperature? Second, the cubic phases form with a variety of lipid degradation products at very small mole fractions of the lipid. Third, the $H_{II}$ lattice unit cell sizes for DOPE-Me degraded DOPE-Me, and DOPE-Me mixed with $\lesssim$2 mol % of representative degradation products are all comparable to within 0.5 Å, suggesting that all these systems have comparable spontaneous curvatures.

The rise in disorder that is apparent in the X-ray diffraction patterns for intermediate $R_0$ systems is concomitant with the appearance of an isotropic $^{31}P$ NMR resonance (see, for example, Figure 10). The class of structures known as lipidic particles also gives rise to the isotropic resonance. [For reviews see Verkleij (1984) and Cullis et al (1985).] Lipidic particles, as well as other complex lipid morphologies that yield isotropic resonances, are clearly evident in freeze-fracture micrographs of DOPE-Me [see, for example, Gagne et al. (1985)]. Lipidic particles are especially prone to occur in mixtures that we would generally identify as intermediate $R_0$ systems, such as the PE–PC mixtures examined by Hui et al. (1983) and Eriksson et al. (1985). It seems likely that high concentrations of lipidic particles, as well as other complex lipid morphologies, are a general feature associated with the disorder readily seen in intermediate $R_0$ systems (Siegel, 1986d).

## Conclusion

From a biological perspective, the mechanisms of $L_\alpha$ to nonbilayer phase transitions have been the subject of much recent attention because these mechanisms have been suggested as being involved in membrane fusion [see Cullis and Hope (1978), Verkleij et al. (1984), Cullis et al. (1985), and Siegel (1986c)]. It is reasonable to suppose that the structures which give rise to at least part of the $^{31}P$ NMR isotropic resonance seen in DOPE-Me mediate the mesomorphic transitions. One must recall, however, that many phospholipid structures are expected to yield the isotropic resonance because on the NMR time scale ($\sim 10^{-5}$ s) a lipid molecule diffusing in the vicinity of a strongly curved lipid monolayer can rotate its long axis through many degrees with respect to the NMR magnetic field (Cullis & de Kruijff, 1979). Indeed, close inspection of freeze-fracture micrographs of DOPE-Me in the vicinity of its transitions yields a multitude of complex structures [see, for example, Figure 4 of Gagne et al. (1985)]. Rather than try to associate given structures with given transition mechanisms, we simply point out that complex lipid structures yielding isotropic resonances appear to be more readily obtained with DOPE-Me than with either DOPE or DOPC. The number of equilibrium phases, as well as the number of nonequilibrium intermediates accessible to DOPE-Me, appears to exceed that of either small or large $R_0$ lipid systems.

If, in fact, a high degree of variability of the lipid monolayer topology is important to biomembranes, then it is reasonable to suppose that living systems will maintain membranes with intermediate, and, perhaps, near constant $R_0$ values, as suggested by Gruner (1985). Conserved $R_0$ values may imply conserved hydrocarbon order parameters when these lipids are constrained to the bilayer organization (Cullis et al., 1986). Especially noteworthy in this regard is the work of Wieslander, Rilfors, Lindblom, and co-workers on the lipid composition of *Acholeplasma laidlawii* A grown under various conditions (Wieslander et al., 1980, 1981a,b, 1986; Rilfors, 1985; Lindblom et al., 1986). They have shown that the organism compensates for adjustment of its environment by regulating the ratio of the predominant lipids, monoglucosyldiglyceride (MGDG) and diglucosyldiglyceride (DGDG). MGDG readily forms $H_{II}$ phases and DGDG forms lamellar phases, so a mixture of the two is analogous, with respect to $R_0$, to DOPE–DOPC mixtures. The regulation has been interpreted in terms of a shape concept. Perhaps the regulatory mechanism can be more quantitatively interpreted, in the same spirit, in terms of $R_0$. For example, if bacteria are grown at various ratios of two fatty acids, so as to vary the lipid composition, do the resultant membranes maintain constant $R_0$ at the growth temperature; i.e., is $d_H$ at the growth temperature, in the presence of dodecane, constant? Although this experiment, to our knowledge, has yet to be performed, the recent study of Lindblom et al. (1986) is highly suggestive. They grew *A. laidlawii* A on various ratios of exogenous palmitic and oleic acid, which resulted in acyl chain compositions of the bacterial membrane lipids that varied from roughly 20 to 95% 18:1c and MGDG:DGDG ratios that varied from 1.70 to 0.18. NMR was used to examine the phase behavior of the total lipid extracts. "It was found for all samples studied...that a phase

transition to either a hexagonal or a cubic phase occurred at about 45–55 °C..." (Lindblom et al., 1986). The remarkable near constancy of the transition temperature over such wide variations in chain and head-group composition suggests that the $R_0$ value of the membrane is actively being held constant by the organism.

This paper describes, by examples with DOPE and its methylated analogues, systems with small, intermediate, and large $R_0$ values. Representative behaviors of each of these categories in excess water as a function of temperature have been shown. To summarize: Small $R_0$ systems (e.g., DOPE) exhibit facile $L_\alpha$–$H_{II}$ transitions over relatively narrow temperature ranges. Such systems are strongly driven to form $H_{II}$ phases. Large $R_0$ systems (e.g., DOPC) are mesomorphically sterile. They have little curvature impetus to form anything other than lamellar phases, at least in excess water and at reasonable temperatures. This attribute of bilayer stability has made large $R_0$ systems, especially phosphatidylcholines, the workhorses of model membrane biophysics. It is a leap of faith to assume that nature, too, generally desires such highly stable lipid bilayers for cell membranes. Intermediate $R_0$ systems (e.g., DOPE-Me) exhibit a rich complexity of structures and behavior over a wide temperature range. The question of which range of $R_0$ nature tends to prefer is straightforwardly answerable, at least in part, by examining the behavior of lipid extracts of biomembranes.

From the perspective of the physical properties of lipid liquid crystals, DOPE-Me is a wonderfully rich material. It exhibits $L_\alpha$, $H_{II}$, and a variety of cubic phases. Moreover, the sequence and characteristic dimensions of these phases seem amenable to simple models and ultimately, we hope, to quantitative characterization of the component free energies that are involved. However, the nonequilibrium and metastable behavior, which is interesting in its own right, is a maze of traps for the unwary experimentalist and calls for special care.

## ACKNOWLEDGMENTS

We thank J. Bentz, H. Ellens, G. Lindblom, A. Parsegian, P. Rand, G. T. Reynolds, J. Seddon, and D. Siegel for helpful discussions during the course of the experiments.

**Registry No.** DOPE, 4004-05-1; DOPE-Me, 96687-23-9; DOPE-$Me_2$, 96687-22-8; DOPC, 4235-95-4; dodecane, 112-40-3.

## REFERENCES

Anderson, D. M. (1986) Ph.D. Thesis, University of Minnesota.

Anderson, D. M., Gruner, S. M., & Leibler, S. (1988) *Proc. Natl. Acad. Sci. U.S.A.* (in press).

Berde, C. B., Anderson, H. C., & Hudson, B. S. (1980) *Biochemistry 19*, 4279–4293.

Boggs, J. M. (1984) *Biomembranes 12*, 3–53.

Brentel, I., Selstam, E., & Lindblom, G. (1985) *Biochim. Biophys. Acta 812*, 816–826.

Brown, P. M., Steers, J., Hui, S. W., Yeagle, P. L., & Silvius, J. R. (1986) *Biochemistry 25*, 4259–4267.

Charvolin, J. (1985) *J. Phys. C 46*, C3-173–C3-190.

Comfurius, P., & Zwaal, R. F. A. (1977) *Biochim. Biophys. Acta 448*, 36–42.

Cullis, P. R., & Hope, M. J. (1978) *Nature (London) 271*, 672–675.

Cullis, P. R., & de Kruijff, B. (1979) *Biochim. Biophys. Acta 559*, 399–420.

Cullis, P. R., Hope, M. J., de Kruijff, B., Verkleij, A. J., & Tilcock, C. P. S. (1985) in *Phospholipids and Cellular Regulation* (Kuo, J. F., Ed.) Vol. 1, CRC Press, Boca Raton, FL.

Cullis, P. R., Hope, M. J., & Tilcock, C. P. S. (1986) *Chem. Phys. Lipids 40*, 127–144.

Deuling, H. J., & Helfrich, W. (1976) *Biophys. J. 16*, 861–868.

Eibl, H. (1977) in *Polyunsaturated Fatty Acids* (Kunau, W. H., & Holman, R. T., Eds.) p 229, American Oil Chemists Society, Champaign, IL.

Eibl, H., & Woolley, P. (1979) *Biophys. Chem. 10*, 261–271.

Ellens, H., Bentz, J., & Szoka, F. C. (1986) *Biochemistry 25*, 4141–4147.

Eriksson, P.-O., Rilfors, L., Lindblom, G., & Arvidson, G. (1985) *Chem. Phys. Lipids 37*, 357–371.

Evans, E., & Metcalfe, M. (1984) *Biophys. J. 46*, 423–426.

Fuller, N., Miller, F., Rand, R. P., & Parsegian, V. A. (1983) *Biophys. J. 41*, 354a.

Gagne, J., Stamatatos, L., Diacovo, T., Hui, S. W., Yeagle, P. L., & Silvius, J. R. (1985) *Biochemistry 24*, 4400–4408.

Gruner, S. M. (1977) Ph.D. Thesis, Princeton University, Princeton, NJ.

Gruner, S. M. (1985) *Proc. Natl. Acad. Sci. U.S.A. 82*, 3665–3669.

Gruner, S. M., Milch, J. R., & Reynolds, G. T. (1982a) *Rev. Sci. Instrum. 53*, 1770–1778.

Gruner, S. M., Barry, D. T., & Reynolds, G. T. (1982b) *Biochim. Biophys. Acta 690*, 187–198.

Gruner, S. M., Cullis, P. R., Hope, M. J., & Tilcock, C. P. S. (1985) *Annu. Rev. Biophys. Biophys. Chem. 14*, 211–238.

Gruner, S. M., Parsegian, V. A., & Rand, R. P. (1986) *Faraday Discuss. 81*, 29–37.

Gutman, H., Arvidson, G., Fontell, K., & Lindblom, G. (1983) in *Surfactants in Solution* (Mittal, K. L., & Lindman, B., Eds.) Vol. 1, pp 143–152, Plenum, New York.

Hauser, H., Pascher, I., Pearson, R. H., & Sundell, S. (1981) *Biochim. Biophys. Acta 650*, 21–51.

Helfrich, W. (1973) *Z. Naturforsch. 28C*, 693–703.

Hui, S. W., Stewart, T. P., Yeagle, P. L., & Albert, A. D. (1981) *Arch. Biochem. Biophys. 207*, 227–240.

Hui, S. W., Stewart, T. P., & Boni, L. T. (1983) *Chem. Phys. Lipids 33*, 113–126.

Hyde, S. T., & Andersson, S. (1985) *Z. Kristallogr. 170*, 225–239.

Hyde, S. T., Andersson, S., Ericsson, B., & Larsson, K. (1984) *Z. Kristallogr. 168*, 213–219.

*International Tables for X-ray Crystallography* (1968) Vol. II, p 147, Kynoch, Birmingham, England.

Israelachvili, J. N., Marcelja, S., & Horn, R. G. (1980) *Q. Rev. Biophys. 13*, 121–200.

Kirk, G. L. (1984) Ph.D. Thesis, Princeton University, Princeton, NJ.

Kirk, G. L., & Gruner, S. M. (1985) *J. Phys. 46*, 761–769.

Kirk, G. L., Gruner, S. M., & Stein, D. L. (1984) *Biochemistry 23*, 1093–1102.

Larsson, K., & Andersson, S. (1986) *Acta Chem. Scand., Ser. B B40*, 1–5.

Larsson, K., Fontell, K., & Krog, N. (1980) *Chem. Phys. Lipids 27*, 321–328.

Lindblom, G., Brentel, I., Stoland, M., Wikander, G., & Wieslander, A. (1986) *Biochemistry 25*, 7502–7510.

Lis, L. J., McAlister, M., Fuller, N., Rand, R. P., & Parsegian, V. A. (1982) *Biophys. J. 37*, 657–666.

Luzzati, V. (1968) in *Biological Membranes* (Chapman, D., Ed.) Vol. I, pp 71–123 Academic, New York.

Luzzati, V., & Husson, F. (1962) *J. Cell Biol. 12*, 207–219.

Luzzati, V., Mariani, P., & Gulik-Krzywicki, T. (1987) in *Physics of Ampiphilic Layers* (Meunier, J., Langevin, D.,

& Boccara, N., Eds.) Springer-Verlag, Berlin.
Mackay, A. L. (1985) *Nature (London) 314*, 604-606.
Marcelja, S. (1976) *Chem. Phys. Lett. 42*, 129-130.
McIntosh, T. J., & Simon, S. A. (1986) *Biochemistry 25*, 4058-4066.
Milch, J. R. (1983) *J. Appl. Crystallogr. 16*, 198-203.
Parsegian, V. A., Fuller, N., & Rand, R. P. (1979) *Proc. Natl. Acad. Sci. U.S.A. 76*, 2750-2754.
Raetz, C. R. H. (1982) in *Phospholipids* (Hawthorne, J. N., & Ansell, G. B., Eds.) pp 435-477, Elsevier Biomedical, Amsterdam.
Rand, R. P. (1981) *Annu. Rev. Biophys. Bioeng. 10*, 277-314.
Reynolds, G. T., Milch, J. R., & Gruner, S. M. (1978) *Rev. Sci. Instrum. 49*, 1241-1249.
Rilfors, L. (1985) *Biochim. Biophys. Acta 813*, 151-160.
Rilfors, L., Lindblom, G., Wieslander, A., & Christiansson, A. (1984) *Biomembranes 12*, 205-245.
Rilfors, L., Eriksson, P.-O., Arvidson, G., & Lindblom, G. (1986) *Biochemistry 25*, 7702-7710.
Schoen, A. H. (1970) *NASA Technical Note D-5541*, National Technical Information Service Document N70-29782, Springfield, VA.
Seddon, J. M., Cevc, G., Kaye, R. D., & Marsh, D. (1984) *Biochemistry 23*, 2634-2644.
Sen, A., & Hui, S. W. (1986) *Biophys. J. 49*, 322a.
Sen, A., Hui, S. W., & Yeagle, P. L. (1986) *Biophys. J. 59*, 434a.
Siegel, D. P. (1986a) *Biophys. J. 49*, 1155-1170.
Siegel, D. P. (1986b) *Biophys. J. 49*, 1171-1183.
Siegel, D. P. (1986c) in *Cell Fusion* (Sowers, A. E., Ed.) Plenum, New York.
Siegel, D. P. (1986d) *Chem. Phys. Lipids 42*, 279-301.
Small, D. M. (1967) *J. Lipid Res. 8*, 551-557.
Tartar, H. V. (1955) *J. Phys. Chem. 59*, 1195-1199.
Tate, M. W., & Gruner, S. M. (1987) *Biochemistry 26*, 231-236.
Tilcock, C. P. S., & Cullis, P. (1982) *Biochim. Biophys. Acta 684*, 212-218.
Verkleij, A. J. (1984) *Biochim. Biophys. Acta 779*, 43-63.
Wieslander, A., Christiansson, A., Rilfors, L., & Lindblom, G. (1980) *Biochemistry 19*, 3650-3655.
Wieslander, A., Rilfors, L., Johansson, L. B. A., & Lindblom, G. (1981a) *Biochemistry 20*, 730-735.
Wieslander, A., Christiansson, A., Rilfors, L., Khan, A., Johansson, L. B. A., & Lindblom, G. (1981b) *FEBS Lett. 124*, 273-278.
Wieslander, A., Rilfors, L., & Lindblom, G. (1986) *Biochemistry 25*, 7511-7517.

# Hydrogen Peroxide Stabilizes the Steroid-Binding State of Rat Liver Glucocorticoid Receptors by Promoting Disulfide Bond Formation†

Emery H. Bresnick,‡ Edwin R. Sanchez,‡ Robert W. Harrison,§ and William B. Pratt*,‡

*Department of Pharmacology, The University of Michigan Medical School, Ann Arbor, Michigan 48109, and Division of Endocrinology and Metabolism, University of Arkansas for Medical Sciences, Little Rock, Arkansas 72205*

*Received October 6, 1987; Revised Manuscript Received December 11, 1987*

ABSTRACT: Hydrogen peroxide and diamide inactivate the steroid-binding capacity of unoccupied glucocorticoid receptors in rat liver cytosol at 0 °C, and steroid-binding capacity is reactivated with dithiothreitol. Treatment of cytosol with peroxide or sodium molybdate, but not diamide, inhibits the irreversible inactivation (i.e., inactivation not reversed by dithiothreitol) of steroid-binding capacity that occurs when cytosol is incubated at 25 °C. Pretreatment of cytosol with the thiol derivatizing agent methyl methanethiosulfonate at 0 °C prevents the ability of peroxide, but not molybdate, to stabilize binding capacity at 25 °C. As derivatization of thiol groups prevents peroxide stabilization of steroid-binding capacity and as treatment with dithiothreitol reverses the effect, we propose that peroxide acts by promoting the formation of new disulfide linkages. The receptor in our rat liver cytosol preparations is present as three major degradation products of $M_r$ 40000, 52000, and 72000 in addition to the $M_r$ 94000 intact receptor. Like the intact receptor, these three forms exist in the presence of molybdate as an 8-9S complex, they bind glucocorticoid in a specific manner, and they copurify with the intact $M_r$ 94000 receptor on sequential phosphocellulose and DNA-cellulose chromatography. Despite the existence of receptor cleavage products, it is clear that peroxide does not stabilize steroid-binding capacity by inhibiting receptor cleavage.

Sulfhydryl groups are required for several functions of the glucocorticoid receptor, including its steroid-binding activity, its transformation[1] from an 8-9S to a 4S form, and the binding of transformed receptors to DNA. Early studies by Rees and Bell (1975) demonstrated a requirement for sulfhydryl groups in maintaining an active steroid-binding conformation of the rat thymocyte glucocorticoid receptor. Other workers have since utilized sulfhydryl derivatizing agents, such as *N*-ethylmaleimide (Formstecher et al., 1984), iodoacetamide

† This investigation was supported by Grant DK31573 from the National Institutes of Health.

* Author to whom correspondence should be addressed.
‡ The University of Michigan Medical School.
§ University of Arkansas for Medical Sciences.

[1] In this work, we will use the word "untransformed" to describe the 8-9S form of the receptor that does not bind to DNA and the word "transformed" to describe the 4S, DNA-binding form.

0006-2960/88/0427-2866$01.50/0 